Cell–cell adhesion in metazoans relies on evolutionarily conserved features of the α-catenin·β-catenin–binding interface

Received for publication, May 9, 2017, and in revised form, July 31, 2017 Published, Papers in Press, August 25, 2017, DOI 10.1074/jbc.M117.795567

Xiangqiang Shao[‡§1], Hyunook Kang[¶1], Timothy Loveless[§‖], Gyu Rie Lee[**], Chaok Seok[**], William I. Weis[‡‡], Hee-Jung Choi[¶], and Jeff Hardin[‡§‖2]

From the [‡]Program in Genetics, [§]Department of Zoology, and [‖]Program in Cellular and Molecular Biology, University of Wisconsin-Madison, Madison, Wisconsin 53706, the Departments of [¶]Biological Sciences and [**]Chemistry, Seoul National University, Seoul 08826, South Korea, and the [‡‡]Departments of Structural Biology and Molecular and Cellular Physiology, Stanford University School of Medicine, Stanford, California 94305

Edited by Eric R. Fearon

Stable tissue integrity during embryonic development relies on the function of the cadherin·catenin complex (CCC). The *Caenorhabditis elegans* CCC is a useful paradigm for analyzing *in vivo* requirements for specific interactions among the core components of the CCC, and it provides a unique opportunity to examine evolutionarily conserved mechanisms that govern the interaction between α- and β-catenin. HMP-1, unlike its mammalian homolog α-catenin, is constitutively monomeric, and its binding affinity for HMP-2/β-catenin is higher than that of α-catenin for β-catenin. A crystal structure shows that the HMP-1·HMP-2 complex forms a five-helical bundle structure distinct from the structure of the mammalian α-catenin·β-catenin complex. Deletion analysis based on the crystal structure shows that the first helix of HMP-1 is necessary for binding HMP-2 avidly *in vitro* and for efficient recruitment of HMP-1 to adherens junctions in embryos. HMP-2 Ser-47 and Tyr-69 flank its binding interface with HMP-1, and we show that phosphomimetic mutations at these two sites decrease binding affinity of HMP-1 to HMP-2 by 40–100-fold *in vitro*. *In vivo* experiments using HMP-2 S47E and Y69E mutants showed that they are unable to rescue *hmp-2*(*zu364*) mutants, suggesting that phosphorylation of HMP-2 on Ser-47 and Tyr-69 could be important for regulating CCC formation in *C. elegans*. Our data provide novel insights into how cadherin-dependent cell–cell adhesion is modulated in metazoans by conserved elements as well as features unique to specific organisms.

Stable intercellular adhesions that maintain tissue integrity are critical for morphogenetic movements during metazoan development (1). Maintaining such adhesions is also important for adult organisms, in which defects can lead to tumorigenesis and metastasis (2, 3). One crucial mediator of intercellular adhesion is the adherens junction, which contains a highly conserved cadherin·catenin complex (CCC).[4] Intercellular adhesions are mediated by the CCC through calcium-dependent homophilic interactions of transmembrane cadherins (4); the intracellular tail of cadherins binds to p120-catenin and β-catenin (5). α-Catenin, which binds to β-catenin, acts as a physical linker connecting the CCC at the membrane to the F-actin cytoskeleton (6–8).

α-Catenin is an actin-binding and -bundling protein consisting of a series of linked α-helical bundles (9–12). The N-terminal domain of mammalian αE- and αN-catenins contains overlapping β-catenin binding and homodimerization sites (7, 13). The C-terminal domain of α-catenin binds to F-actin (the actin-binding domain) (6, 14). The middle (M) domain of α-catenin is composed of three four-helix bundles designated M1, M2, and M3 (11). The central two helices of the M1 bundle contain the vinculin-binding site (15, 16). These helices dissociate or "unfurl" from the bundle to bind vinculin. This unfurling is inhibited by the M3 bundle, but mechanical tension alters the relative positions of the M subdomains to enable vinculin binding, which further strengthens the CCC–F-actin linkage (11, 12, 15, 17, 18).

α-Catenin is recruited to the CCC by β-catenin. Via its central armadillo (Arm) repeats, β-catenin binds the highly conserved intracellular domain of E-cadherin, and the interaction is strengthened by phosphorylation of a serine-rich region in cadherin (19–22). The region of β-catenin N-terminal to the Arm repeats binds to the N-terminal domain of α-catenin (23, 24). *In vitro* reconstitution of the CCC demonstrates that these

This work was supported under the framework of the International Cooperation Program managed by National Research Foundation of Korea Grant 2015K2A1A2070030 (to H. J. C.), National Research Foundation of Korea Grant NRF-2016R1A2B4013488 (to H. J. C.) funded by the Korean government (Ministry of Science, ICT, and Future Planning), Creative-Pioneering Researchers Program through Seoul National University (to H. J. C.), and National Institutes of Health Grants GM094663 and GM114462 (to W. I. W.) and GM058038 (to J. H.). The authors declare that they have no conflicts of interest with the contents of this article. The content is solely the responsibility of the authors and does not necessarily represent the official views of the National Institutes of Health.

This article contains supplemental Figs. S1–S11.

The atomic coordinates and structure factors (code 5XA5) have been deposited in the Protein Data Bank (http://wwpdb.org/).

[1] Both authors contributed equally to this work.

[2] To whom correspondence may be addressed: School of Biological Sciences, Seoul National University, Seoul 08826, South Korea. Tel.: 82-2-880-6605; Fax: 82-2-872-1993; E-mail: choihj@snu.ac.kr.

[3] To whom correspondence may be addressed: Dept. of Integrative Biology, University of Wisconsin-Madison, Madison, WI 53706. Tel.: 608-262-9634; Fax: 608-262-7319; E-mail: jdhardin@wisc.edu.

[4] The abbreviations used are: CCC, cadherin-catenin complex; TEV, tobacco etch virus; SEC, size-exclusion chromatography; MALS, multiangle light scattering; ITC, isothermal titration calorimetry; PDB, Protein Data Bank.

three proteins form a stable complex (25). Although binding to β-catenin weakens the affinity of αE-catenin for F-actin in solution (26, 27), αE-catenin maintains association with both of these binding partners when tension is applied to the complex (8). Previous structural studies of αE- and αN-catenin indicate that α-catenin interacts with β-catenin mainly via its N-terminal four-helix bundle (N1 bundle), which is bridged to the second four-helix bundle (N2 bundle) by one continuous α helix (α4). The two four-helix bundles of α-catenin move with respect to each other to accommodate insertion of an α helix from β-catenin (13). Whether these N1 interactions and structural changes in the N domain are evolutionarily conserved has not been established nor has the functional significance of these interactions been examined in an *in vivo* setting.

Another feature of adherens junctions *in vivo* is their ability to assemble, disassemble, and reassemble dynamically during morphogenesis (28). Because post-translational modifications to the cadherin·catenin complex are known to modulate the ability of CCC components to bind one another (19, 20, 29–34), such modifications represent a potential mechanism for regulating junctional stability. In particular, perturbing phosphorylation of key residues in E-cadherin and β-catenin has been shown to alter adhesion in cultured cells (35–38) and to modify junctional morphology during embryonic development (19, 39, 40).

Phosphoregulation of the β-catenin·α-catenin association has been less well-studied. Phosphorylation on Tyr-142 of vertebrate β-catenin inhibits its ability to bind α-catenin (30, 32, 41). The β-catenin residue Tyr-142 is a target of multiple kinases, including Fer and Fyn, that are recruited to adherens junctions by p120-catenin (32). Accordingly, a phosphomimetic Y142E transgene added to cells that lack endogenous β-catenin does not confer adhesion in cultured mouse cells (42), and Tyr-142 phosphorylation by focal adhesion kinase increases vascular permeability and the accompanying junctional breakdown in vascular endothelial cells (43). Although the effects on CCC-mediated adhesion play a role in both phenotypes, Tyr-142 phosphorylation of β-catenin also increases its nuclear localization and ability to participate in transcriptional coactivation (30, 41), which limits the interpretation of these experiments. Moreover, the role of these residues in regulating the α-catenin/β-catenin interaction during embryonic morphogenesis has not been assessed. Protein kinase D1 (PKD1) has been shown to phosphorylate β-catenin at Thr-120 in cultured cells, resulting in decreased nuclear β-catenin localization and transcriptional function (44) and increased plasma membrane and trans-Golgi network localization (45, 46). The significance of phosphorylation of Thr-120 for association with α-catenin and its role in an intact organism have not been examined.

Caenorhabditis elegans provides a unique model to explore evolutionary conservation of mechanisms that mediate the α-catenin·β-catenin– binding interface and to probe requirements for elements of that interface *in vivo*. *C. elegans* has conserved homologs of each component of the CCC as follows: HMR-1/cadherin, HMP-2/β-catenin, and HMP-1/α-catenin (47, 48). Moreover, HMP-1 is the sole α-catenin homolog in *C. elegans,* removing any issues of redundancy. In addition, HMP-2 does not normally play a role in the nucleus, and its functions are restricted to the CCC, simplifying interpretation of experiments involving β-catenin.

Our results show that the HMP-1·HMP-2 complex adopts a five-helix bundle structure. Deleting the first α helix within the HMP-1 N domain reduces its ability to bind HMP-2. We also show that phosphomimetic substitutions at HMP-2 Ser-47 or HMP-2 Tyr-69, which are homologous to β-catenin Thr-120 and Tyr-142, respectively, decrease its binding to HMP-1. These studies test requirements for key elements within α- and β-catenin in maintaining their strong association during morphogenetic events *in vivo*. Our results highlight structurally diverse yet biologically convergent evolutionary solutions that metazoans have adopted to stabilize the α-catenin·β-catenin association, which is crucial in all multicellular organisms.

Results

HMP-1 N1 domain is required to suppress the latent ability of HMP-1 to form homodimers

C. elegans HMP-1/α-catenin and HMP-2/β-catenin contain key conserved features found in their vertebrate counterparts (Fig. 1*A* and supplemental Figs. S1 and S2). Morphogenesis of the *C. elegans* embryo requires adherens junctions to be capable of withstanding substantial tensile forces (48–50), so we compared the binding affinity of HMP-1 and HMP-2 to their vertebrate counterparts to see whether there are features of the worm complex that reflect adaptation to such physical demands. HMP-1/α-catenin is homologous to mammalian α-catenin, consisting of the N-terminal HMP-2/β-catenin-binding domain, M domain, and the C-terminal actin-binding domain (Fig. 1*A*). The N-terminal regions of αE-catenin and αN-catenin are responsible for homodimerization as well as β-catenin binding; they form either homodimers or heterodimers with β-catenin (7, 13, 51). Previously, native gel-shift data showed that unlike αE-catenin, HMP-1 is present as a monomer in solution even after a 1-h incubation at 25 °C (49). Here, we confirmed that purified HMP-1 is homogeneously monomeric in solution by multiangle light scattering (MALS) (Fig. 1*B*), and we showed that HMP-1 remains monomeric even after overnight incubation at 28 °C at a concentration of 80 μM (Fig. 1*C*). To test whether HMP-1 has latent potential to form a dimer, we made a construct that deletes 70 amino acids at the N terminus (HMP-1NΔ70), which corresponds to a dimeric αE-catenin construct (αE-catNΔ81 (7)), and we identified the oligomeric state of this mutant by gel-filtration chromatography. Similar to αE-catNΔ81, HMP-1NΔ70 was predominantly dimeric in solution even at 10 μM and at 4 °C (Fig. 1*C*), suggesting that the third and fourth helices of HMP-1 N1 can form a homodimer if the HMP-1 N1 bundle is disassembled. Because wild-type HMP-1 is a monomer, these results imply that the HMP-1 N1 forms a more stable four-helix bundle than that in αN- and αE-catenins.

Monomeric forms of αN- and αE-catenins have similar affinity toward β-catenin, with dissociation constants in the range of 15–25 nM (13). HMP-1 was recently shown to interact with the β-catenin homolog, HMP-2, with K_d of ~1 nM (52), but its minimal binding site with full affinity has never been studied.

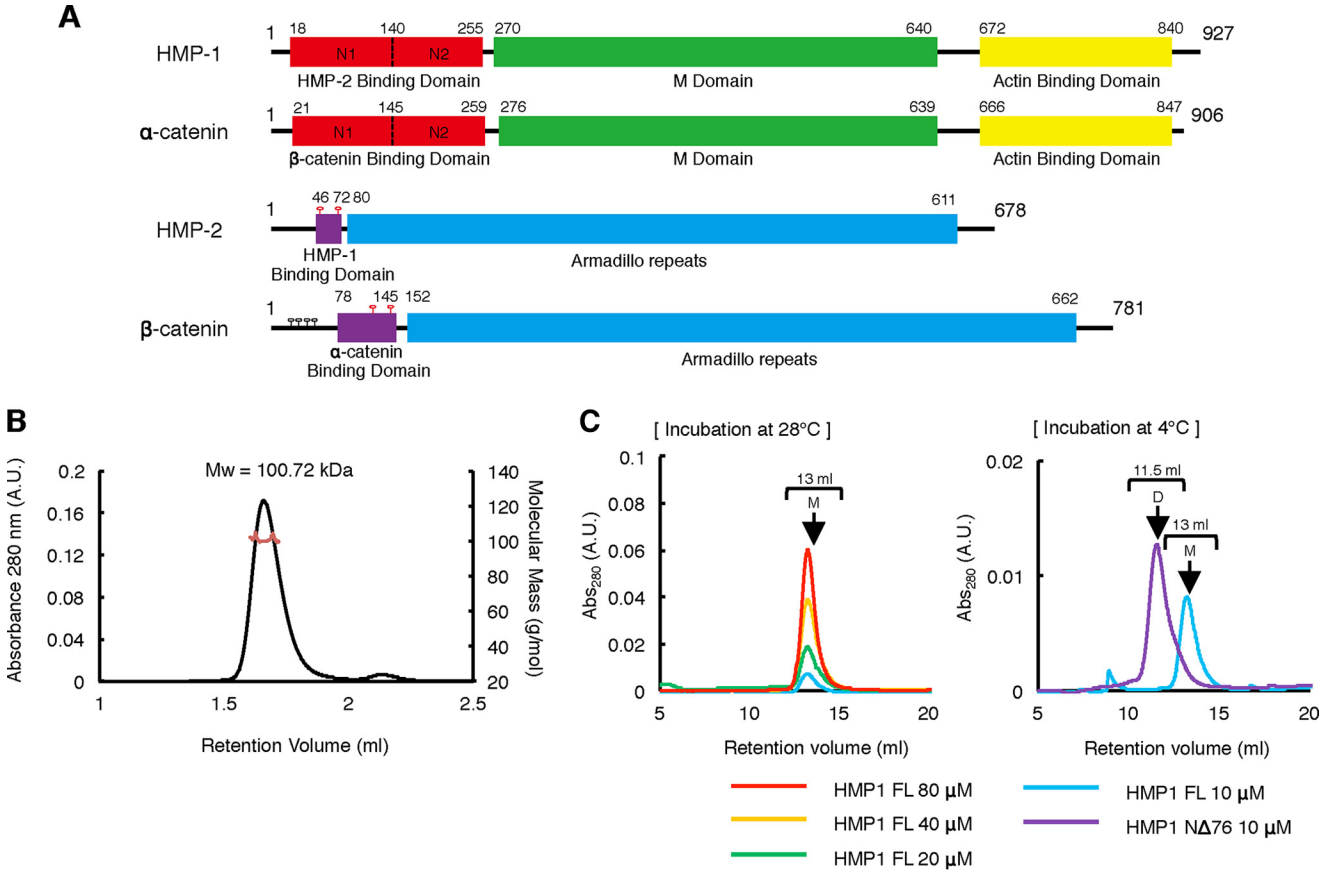

Figure 1. Domain structures of HMP-1/α-catenin and HMP-2/β-catenin and oligomeric state of HMP-1. *A,* comparison of the domain organization of HMP-1 and α-catenin and HMP-2 and β-catenin. In HMP-1 and α-catenin, *red* = HMP-2/β-catenin-binding domain; *green* = M domain; and *yellow* = F-actin-binding domain. In HMP-2 and β-catenin, *purple* = HMP-1/α-catenin-binding domain and *blue* = armadillo repeats. Residue numbers of the termini of each domain are shown. Phosphosites of HMP-2 and β-catenin are marked with a *ball on stick symbol*. The N-terminal phosphosites of β-catenin are colored *black*, and conserved phosphosites within the HMP-1/α-catenin-binding site are colored *red*. *B,* monomeric state of HMP-1 confirmed by *MALS*. Elution profile and the calculated molecular mass are shown. *A.U.,* absorbance units. *C,* overlay of SEC profiles of HMP-1 at 10, 20, 40, and 80 μM concentrations after 1 h of incubation at 28 °C is shown on the *left*. On the *right*, an overlay of SEC profiles of HMP-1NΔ70 and full-length HMP-1 is shown. *M* and *D* represent monomer and dimer, respectively.

We performed isothermal titration calorimetry (ITC) measurements using several different constructs of HMP-1 and HMP-2 (Table 1 and supplemental Fig. S3). Full-length HMP-1 and the isolated HMP-1 N domain (HMP-1N) show similar affinity to HMP-2 (HMP-2(13–678)), confirming that the N domain is responsible for HMP-2 binding.

The first structural view of the αE-catenin/β-catenin interaction was obtained through a βα-catenin chimeric protein in which amino acids 118–151 of β-catenin were included (13). However, recent biochemical and structural results indicate that a more extended N-terminal fragment of β-catenin, up to residue 78, is required for full binding affinity to αN-catenin, with residues 85–99 of β-catenin forming an additional α helix that interacts with the N-terminal region of αN-catenin (13). Sequence alignment of HMP-2 and β-catenin shows that residues 89–100 of β-catenin are conserved in HMP-2 (residues 19–30) (supplemental Fig. S4). To test whether these residues in HMP-2 are required for full affinity binding to HMP-1, we performed affinity measurements using an HMP-2 construct lacking the N-terminal 35 amino acids (HMP-2(36–678)). In contrast to mammalian β-catenin, deletion of these residues did not decrease affinity for HMP-1 (Table 1). To determine the minimal HMP-1-binding region within HMP-2, we expressed HMP-2 residues 36–79 (HMP-2(36–79)), which correspond to β-catenin residues 106–152, as a GST fusion protein and used it for ITC experiments. HMP-2(36–79) bound to HMP-1 with a K_d of 3 nM, essentially the same as the affinity of full-length HMP-2 for HMP-1. Interestingly, the 1 nM affinity of the interaction between HMP-1 and HMP-2(36–678) is 315-fold higher than between the corresponding constructs from α- and β-catenin (amino acids 96–781) and 20-fold higher than the affinity between full-length α- and β-catenins (13).

Helix α1 of HMP-1 is crucial for formation of the HMP-1·HMP-2 complex

To understand the high-affinity interaction between HMP-1 and HMP-2, we determined a crystal structure of the HMP-1·HMP-2 complex. We purified the complex of HMP-1(2–274) and HMP-2(36–79), the minimal regions required for full binding affinity, crystallized it, and determined its structure at 1.6 Å resolution. The structure reveals that the four helices of the HMP-1 N1 subdomain rearrange to accommodate a single α helix formed by HMP-2 residues 46–69, forming a five-helix bundle (Fig. 2*A*). Structural alignment of HMP-1 with the unbound αN-catenin monomer shows that the position of α1 is almost identical in both structures but that helices α2 and α3 are located in different positions (Fig. 2*B*) and are repositioned upon HMP-2 binding; the α1 helix, which makes direct con-

Table 1
ITC measurement of HMP-1 binding to HMP-2

Proteins		K_D	ΔH	$T\Delta S$	ΔG
		nM	kcal mol^{-1}	kcal mol^{-1}	kcal mol^{-1}
HMP-1	HMP-2 (13–678)	1.0 ± 0.4	−21.4 ± 0.6	−9.1	−12.3
HMP-1N	HMP-2 (13–678)	1.0 ± 0.08	−17.7 ± 0.3	−5.4	−12.3
HMP-1N	HMP-2 (36–678)	1.0 ± 0.02	−16.4 ± 0.4	−4.1	−12.3
HMP-1N	GST-HMP-2 (36–79)	2.9 ± 0.3	−11.8 ± 0.1	−0.2	−11.6
HMP-1NΔ44	HMP-2 (36–678)	2200 ± 340	−5.4 ± 0.2	2.3	−7.7
HMP-1N (Q27L/E31V)	HMP-2 (13–678)	24 ± 9	−12.7 ± 0.3	−2.3	−10.4

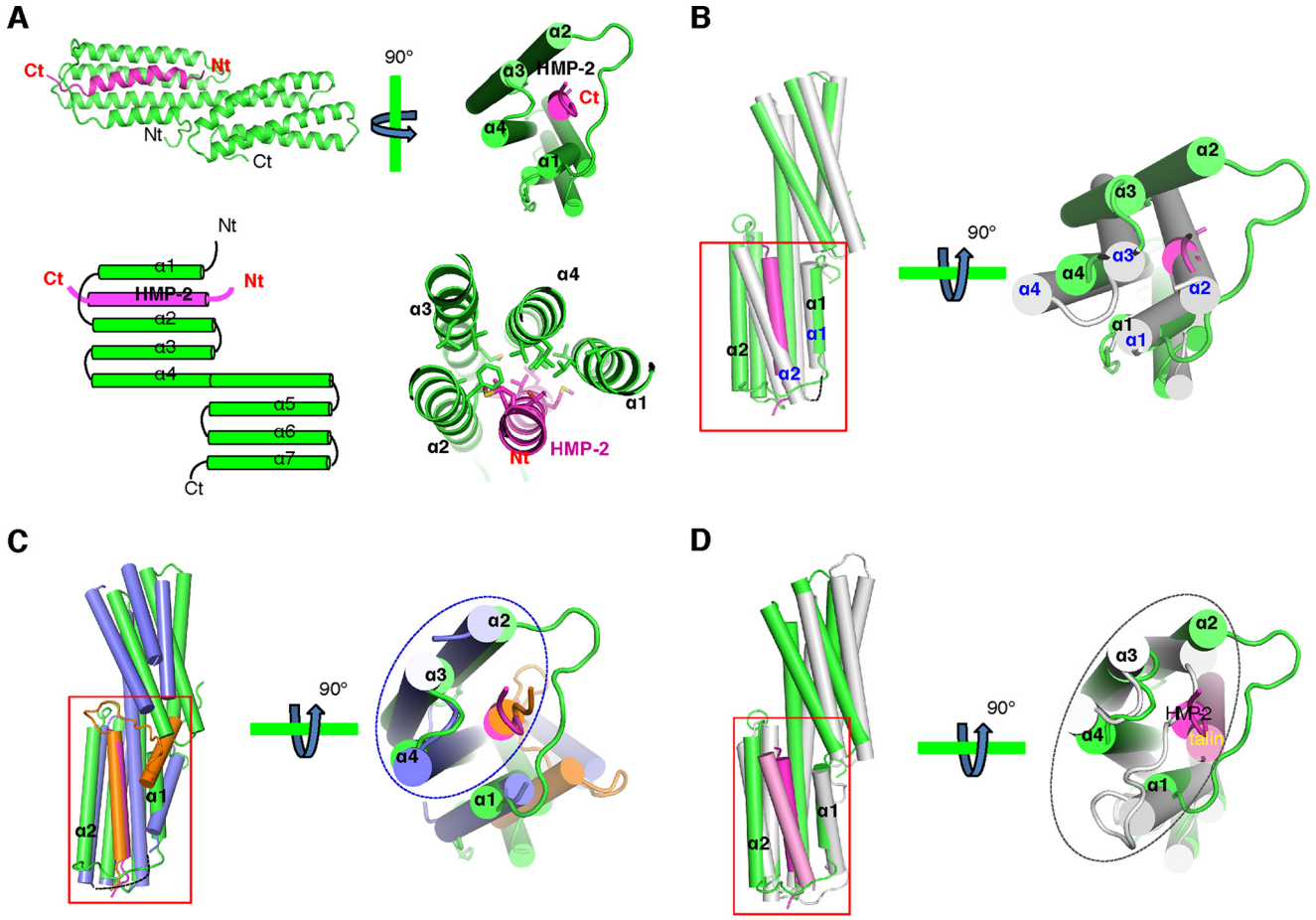

Figure 2. Crystal structure of HMP-1·HMP-2 complex and structural comparison with αN-catenin·β-catenin complex and αN-catenin. *A,* overall structure of the HMP-1N·HMP-2(37–79) complex. Helices α1–α7 of HMP-1 are colored *green* and labeled; the HMP-2 helix is colored *magenta*. Hydrophobic residues forming a five-helix bundle are shown as *sticks*. *B,* monomeric αN-catenin (PDB code 4P9T) and HMP-1·HMP-2 complex compared by superposition of N2 bundles. HMP-1 and HMP-2 helices are colored as in *A*. αN-catenin is shown in *gray*. *C,* top and side views of the HMP-1·HMP-2 complex structure aligned with the αN-catenin·β-catenin complex structure (PDB code 4ONS). αN-catenin and β-catenin helices are colored *blue* and *orange*, respectively. *D,* vinculin·talin complex (PDB code 1T01) and HMP-1·HMP-2 complex compared by superposition of N1 bundles. Vinculin and talin are colored *gray* and *light pink*, respectively.

tacts with the N2 bundle and the α4 helix, remains stationary. The 11-amino acid linker between the HMP-1 α1 and α2 helices is long enough to accommodate the structural rearrangement from a four- to five-helix bundle upon HMP-2 binding. The C-terminal region of the HMP-2 helix interacts with the linker. Although this linker conformation is stabilized by crystal contacts in our structure (supplemental Fig. S5), computational analysis suggests that these interactions exist in the absence of crystal contacts (supplemental Fig. S6).

The HMP-1·HMP-2 structure revealed similarities and differences with the mammalian αN-catenin·β-catenin structure. The five-helix bundle formed by HMP-1 and HMP-2 contrasts with the situation in the αN-catenin·β-catenin complex, where β-catenin forms a four-helix bundle with αN-catenin N1 helices 2–4; the displaced αN-catenin α1 helix packs on the outside of the new four helix bundle, against the β-catenin helix. The α1 helix also packs against a second β-catenin helix formed by residues 85–96, which causes bending of N2 bundle to avoid steric clashes (Fig. 2*C*) (13). In the HMP-1·HMP-2 five-helix bundle, HMP-2 makes non-polar contacts predominantly with HMP-1 helices α1, α2, and α4, and the interactions with α2 and α4 are conserved in the mammalian structures (Fig. 3*A*). There are also polar interactions mediated by residues in HMP-1 helix α1 and HMP-2 that are not conserved in the mammalian homologs. Specifically, residues Gln-27 and Glu-31 of HMP-1, which form hydrogen bonds with Gln-57 and Lys-60 of HMP-2, correspond to residues Leu-31 and Val-35 of αN-catenin, respectively (Fig. 3*B*). The HMP-1 mutant Q27L/E31V binds to

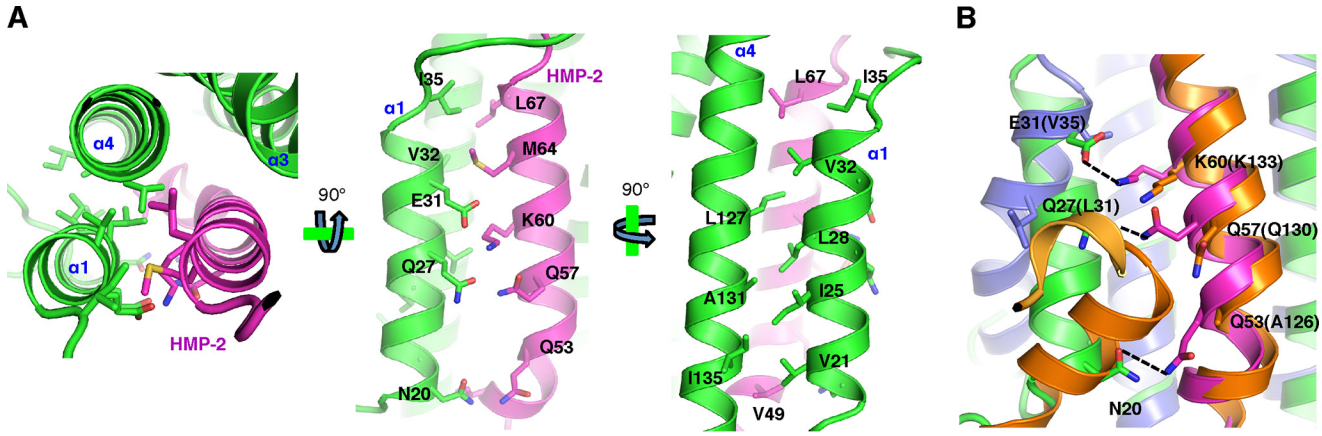

Figure 3. Key interactions of the α1 helix of HMP-1 with HMP-2. *A,* interacting residues of HMP-1 helix α1 with HMP-2 and HMP-1 helix α4 (within 3.6 Å) are shown as *sticks* and labeled. *B,* comparison of the interactions between HMP-1 helix α1 and HMP-2 and those between the corresponding regions of αN-catenin and β-catenin. Residues 100–103 of β-catenin, which form a 3_{10} helix, are represented as a *light orange helix*. Polar interactions between HMP-1 helix α1 and HMP-2 are shown as *dashed lines*. Each residue involved in the interaction is labeled, and the corresponding residue in αN-catenin and β-catenin is shown in *parentheses*.

HMP-2 with an affinity of 24 nM (Table 1 and supplemental Fig. S3), comparable with the affinity of mammalian α-catenin for β-catenin. Thus, these additional polar interactions appear to contribute to the higher affinity between HMP-1 and HMP-2 relative to α- and β-catenin.

Remarkably, the change from a four- to five-helix bundle is very similar to that binding of talin to vertebrate vinculin, which is a paralog of α-catenin (53, 54). Superposition of the HMP-1·HMP-2 complex with those of vinculin·talin (*e.g.* PDB codes 1T01 and 1RKC) reveals very similar structures (Fig. 2*D*).

To test the importance of helix α1 to the affinity of HMP-1 for HMP-2, we made an α1 deletion mutant (HMP-1(NΔ44)). We found that the solubility of HMP-1(NΔ44) was much lower than wild-type HMP-1N, likely because hydrophobic residues on helix α2 are exposed to solvent by dimerization. Indeed, the gel-filtration profile of HMP-1NΔ44 suggested it dimerizes (supplemental Fig. S7). Although HMP-1NΔ44 does bind to HMP-2, the affinity was decreased dramatically by more than 2000-fold (K_d of 2.2 μM; Table 1), indicating that helix α1 is essential for tight binding of HMP-1 to HMP-2.

We also evaluated the effects of HMP-2 binding on HMP-1 stability. First, we measured the melting temperature (T_m) of the HMP-1 N domain in the absence and presence of HMP-2 using circular dichroism (CD) spectroscopy. Unexpectedly, HMP-1 N showed two transitions, one at 42 °C and the other at 67 °C, implying separate melting of the two bundles (Fig. 4*A*). In contrast, the HMP-1·HMP-2 complex has a single transition at 55 °C, with no obvious second transition, although the CD signal changes slightly around 98 °C. The shift of the initial transition to a higher temperature when bound to HMP-2 could imply a more stable structure. This was tested by limited proteolysis using endoproteinase GluC, which selectively cleaves peptide bonds C-terminal to glutamic acid residues. When the HMP-1 and the HMP-1·HMP-2 complex were incubated with GluC under the same conditions, more digestion was observed in HMP-1 alone (Fig. 4*B*), although only 2 of 14 possible cleavage sites are located close to HMP-2 in the complex. Interestingly, one cleavage site is present at the linker between the α1 and α2 helices, and in the absence of HMP-2, this site could be cleaved readily, which may reflect lower stability.

Helix α1 of HMP-1 is crucial for mediating HMP-1·HMP-2 association in vivo

The HMP-1·HMP-2 complex structure and ITC data showed that HMP-1 helix α1 has a crucial role in the HMP-1/HMP-2 interaction. Our previous *in vivo* work showed that deleting the entire β-catenin-binding domain at the HMP-1 N terminus completely abolishes the ability of HMP-1 to bind to HMP-2 (49). However, the importance of the HMP-1 helix α1 to the interaction with HMP-2 has never been examined *in vivo*. HMP-1::GFP localizes predominantly at junctions in elongating wild-type embryos (Fig. 5*A*) and is able to fully rescue *hmp-1*(*zu278*) mutants (Fig. 5*B*). In contrast, when expressed in a wild-type background, much more HMP-1Δα1::GFP (HMP-1Δ2–44::GFP) is found in the cytoplasm compared with full-length HMP-1::GFP (Fig. 5, *C* and *E*), suggesting that HMP-1 helix α1 is important for mediating binding between HMP-1 and HMP-2. Interestingly, HMP-1Δα1::GFP is still able to rescue *hmp-1*(*zu278*) mutants (Fig. 5*D*), although rescue efficiency is not as high as for full-length HMP-1::GFP, even though both transgenes express at similar levels (supplemental Fig. S8): full-length HMP-1::GFP rescues *hmp-1*(*zu278*) mutants with an efficiency of 100%, whereas HMP-1Δα1::GFP rescues *hmp-1*(*zu278*) at 57.8% efficiency. This suggests that the weak binding between HMP-1Δα1 and HMP-2 might still be sufficient for some *in vivo* functions. Consistent with its weak junctional recruitment, the half-life of recovery of HMP-1 in fluorescence recovery after photobleaching (FRAP) analysis was greatly increased in HMP-1Δα1::GFP ($t_{1/2}$ = 18.16 ± 3.57 s, n = 5) compared with wild type ($t_{1/2}$ = 7.34 ± 2.18 s, n = 5; significantly different, p = 0.03, Student's t test; supplemental Fig. S9). These data are consistent with a greatly diminished ability of HMP-1 to bind to HMP-2 when it lacks helix α1.

Deleting any of the helices α2, α3, and α4 should affect the overall structural stability of HMP-1, and it would be expected to abolish its binding to HMP-2. Consistent with this prediction, constructs carrying deletions of each of the remaining α-helices (α2, α3, and α4) all failed to rescue *hmp-1*(*zu278*) mutants (supplemental Fig. S10).

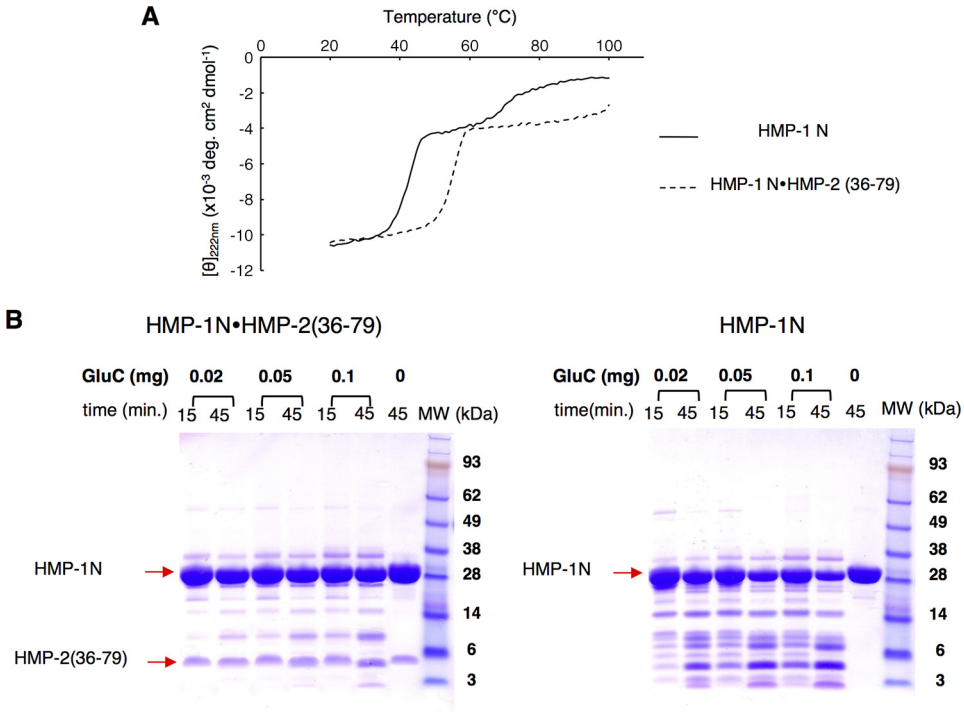

Figure 4. Increased structural stability of HMP-1N upon HMP-2 binding. *A,* melting curves of HMP-1N and the HMP-1N·HMP-2(36–79) complex were measured by circular dichroism spectrometry. *B,* proteolytic digestion of HMP-1N and the HMP-1N·HMP-2(36–79) complex by endoGluC are shown. Amount of endoGluC added in each reaction is shown above the gel; samples were taken from each reaction after 15 and 45 min.

In summary, the detailed functional analysis we performed, based on the HMP-1·HMP-2 complex structure, confirmed a key role for helix α1 of an α-catenin for the first time *in vivo*.

Key phosphorylatable residues are required for the HMP-1/HMP-2 interaction in vitro

HMP-2, unlike vertebrate β-catenin, only functions as a cell adhesion molecule and is not involved in Wnt signaling under normal conditions (55–57). HMP-2 retains internal, conserved potential phosphosites, however, so we were curious as to whether HMP-2 Ser-47 and Tyr-69, which correspond to Thr-120 and Tyr-142 of β-catenin, respectively, and lie at the termini of the binding surface between HMP-1 and HMP-2 (Fig. 6*A*), could regulate the interaction of HMP-2 with HMP-1. To test this possibility, we made four different HMP-2 mutants, S47A and Y69F (non-phosphorylatable mutants) and S47E and Y69E (phosphomimetic mutants), and measured their affinity for HMP-1 by ITC (supplemental Fig. S11).

As shown in Table 2, the two non-phosphorylatable mutants (S47 and Y69F) did not show any difference in binding affinity for HMP-1, with a K_d of ~1 nM. The phosphomimetic mutants (S47E and Y69E), however, showed a dramatically decreased binding affinity for HMP-1. The S47E mutant shows ~40-fold reduced affinity to HMP-1, which could be caused by charge repulsion with Asp-141 of HMP-1 as well as Glu-50 of HMP-2 (Fig. 6*B*). The affinity of the HMP-2 Y69E mutant for HMP-1 was reduced by 100-fold, which is likely caused by introduction of a charged residue at the hydrophobic core (Fig. 6*C*). Given the solvent exposure of the Tyr-69 OH group, it is possible that a Glu substitution has other consequences, such as effects on packing interactions; nevertheless, these results are consistent with a role for pSer-47 and pTyr-69 in negative regulation of the binding of HMP-2 to HMP-1.

Conserved phosphorylation sites in HMP-2 are crucial in vivo

The role of putative phosphoresidues (Thr-120 and Tyr-142 in vertebrate β-catenin) in regulating the binding of β-catenin to α-catenin has not been tested in a living organism. To ascertain whether the analogous residues in *C. elegans* (Ser-47 or Tyr-69 in HMP-2) might regulate CCC function *in vivo*, phosphomimetic and phospho-null mutants were made at each position. The pattern of junctional localization of all phosphomutant proteins was indistinguishable from wild-type HMP-2::GFP (Fig. 7, *A* and *B*). Non-phosphorylatable constructs were able to rescue *hmp-2*(*zu364*) mutants to viability and were maintained as homozygous lines (Fig. 7*A*). Lethality in the HMP-2(S47A)::GFP and HMP-2(Y69F)::GFP lines was 52.2% (n = 782 embryos) and 50.1% (n = 305), respectively, similar to wild-type HMP-2::GFP (53.9%, n = 178). In contrast, phosphomimetic HMP-2(S47E)::GFP and HMP-2(Y69E)::GFP constructs completely failed to rescue *hmp-2*(*zu364*); homozygous mutants expressing these transgenes die with the Hmp phenotype and are indistinguishable from homozygous mutants lacking the transgene (Fig. 7*B*).

We then performed immunostaining to assess HMP-1 distribution in *hmp-2*(*zu364*) mutants expressing mutant HMP-2::GFP constructs (Fig. 8*A*). HMP-1 localizes predominantly to junctions in *hmp-2*(*zu364*) embryos rescued by non-phosphorylatable HMP-2(S47A)::GFP and HMP-2(Y69F)::GFP, similar to those rescued by wild-type HMP-2::GFP. However, in the dead *hmp-2*(*zu364*) embryos expressing phosphomimetic HMP-2(S47E)::GFP and HMP-2(Y69E)::GFP, HMP-1 is much more cytoplasmic compared with embryos expressing wild-

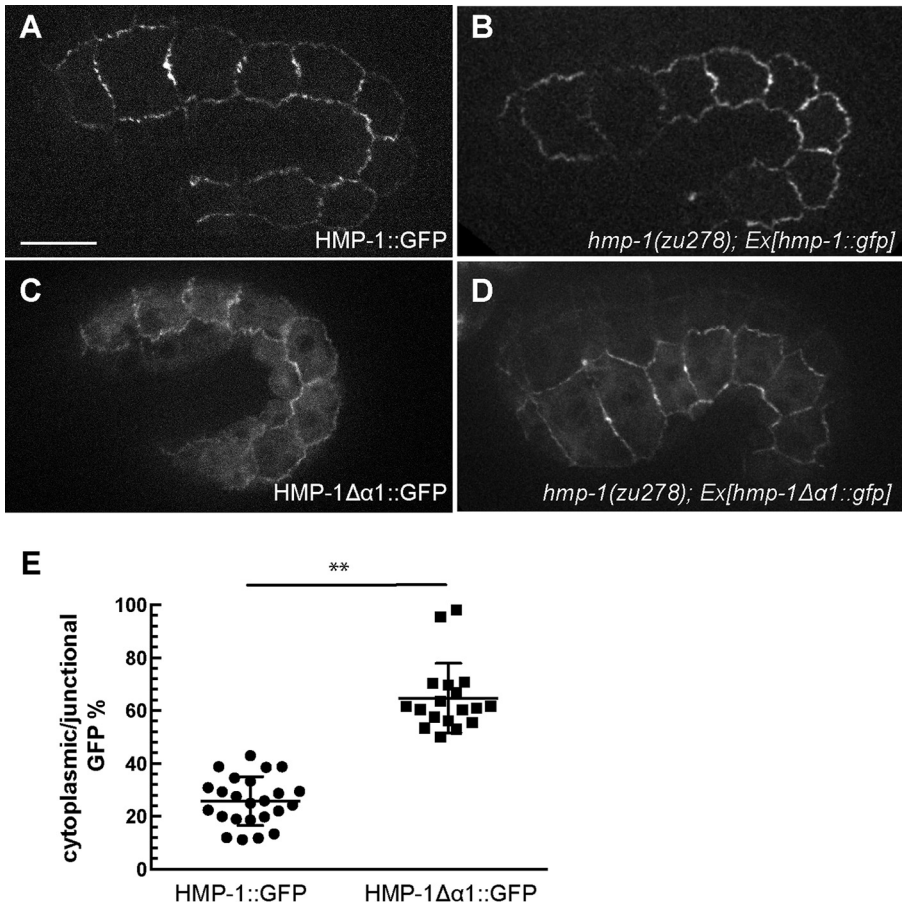

Figure 5. HMP-1 helix α1 is crucial for mediating the HMP-1/HMP-2 interaction *in vivo*. *A,* full-length HMP-1::GFP localizes predominantly at junctions in wild-type embryos. *B,* full-length HMP-1::GFP fully rescues *hmp-1*(*zu278*) mutants. *C,* HMP-1Δα1::GFP exhibits more cytoplasmic expression compared with full-length HMP-1::GFP, suggesting decreased binding affinity for HMP-2. *D,* HMP-1Δα1::GFP still retains ability in rescuing *hmp-1*(*zu278*) mutants. *Scale bar,* 10 μm. *E,* quantitative analysis of cytoplasmic/junctional localization of full-length HMP-1::GFP and HMP-1Δα1::GFP (indicated as a percentage). HMP-1Δα1::GFP shows significantly greater cytoplasmic signal compared with HMP-1::GFP. **, $p \leq 0.01$; Student's *t* test.

type HMP-2::GFP. These results are consistent with the ITC results and indicate reduced recruitment of HMP-1 by the phosphomimetic mutant HMP-2:GFP proteins *in vivo* (Fig. 8*B*).

We next performed FRAP analysis on rescued embryos to assess junctional HMP-2 dynamics. The half-life of recovery was significantly increased for each of the HMP-2 phospho-null constructs (HMP-2(S47A)::GFP and HMP-2(Y69F)::GFP) ($t_{½}$ = 22.22 ± 2.38 s for S47A (n = 6) and 21.32 ± 2.67 s for Y69F (n = 8) compared with wild type ($t_{½}$ = 9.68 ± 1.01 s, n = 6); significantly different, $p \leq 0.01$, Student's *t* test; supplemental Fig. S9). Lethality of *hmp-2*(*zu364*) mutants carrying phosphomimetic constructs precluded acquisition of FRAP data in those lines. The increased half-life of recovery for HMP-2 phospho-null mutants suggests that phosphorylation of HMP-2 Ser-47 and Tyr-69 could regulate its junctional dynamics *in vivo*.

Discussion

α-Catenin·β-catenin– binding interface exhibits evolutionary diversity but functional convergence

Structural, biochemical, and *in vivo* studies of HMP-1/α-catenin in *C. elegans* provide a unique opportunity to assess structural diversity yet functional conservation of the α-catenin·β-catenin– binding interface in metazoans. There is a basic similarity of the α-catenin/β-catenin interaction across the animal kingdom; HMP-2/β-catenin forms an amphipathic helix that packs into the HMP-1/α-catenin N1 bundle. However, the overall architecture of the worm and mammalian complex differs; the *C. elegans* complex involves converting the NI four-helix bundle into a five-helix bundle, whereas the α1 helix in mammalian α-catenin is displaced from the bundle and instead contributes to the interaction by binding along the outside of the bundle and forms additional contacts with another β-catenin helix that is absent in HMP-2.

The similarity of the five-helix bundles in the HMP-1·HMP-2 and vertebrate vinculin·talin complexes is consistent with the evolution of these two proteins from a common ancestor. The differences in the architecture of these complexes with that of the mammalian α-catenin·β-catenin complex likely reflects further divergence of α-catenin and vinculin functions during the evolution of more complex tissue architectures.

The structural features of the HMP-2·HMP-1 complex may also explain differences we recently noted in the binding affinities of these two proteins compared with their vertebrate counterparts. Whereas E-cadherin binding to β-catenin increases the affinity of β-catenin for α-catenin, with K_d of ~1 nM (13), which is similar to the affinity between HMP-1 and HMP-2, we recently found that binding of HMR-1, an E-cadherin homolog, did not change the affinity of HMP-2 for HMP-1 (52). This

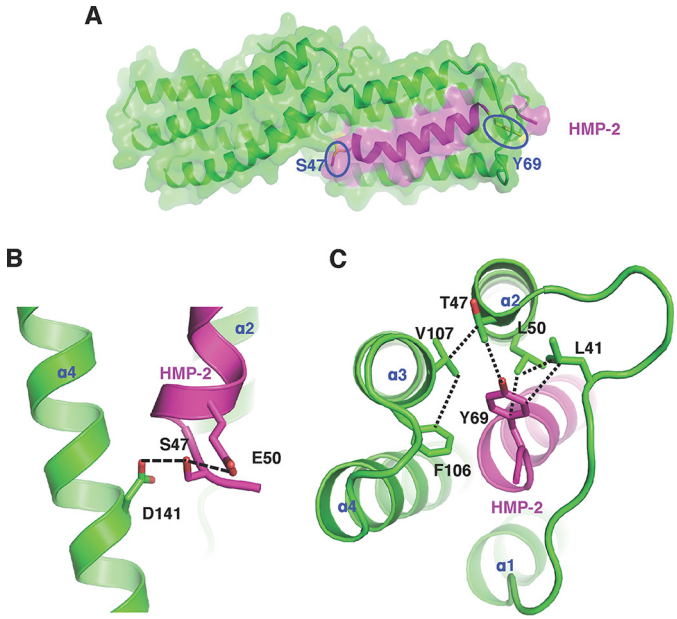

Figure 6. Ser-47 and Tyr-69 of HMP-2 are positioned at the N- and C-terminal ends of the HMP-2 helix in the HMP-1·HMP-2 complex. *A,* Ser-47 and Tyr-69 of HMP-2 are represented as *sticks* on the surface model of the HMP-1·HMP-2 complex. *B,* close contacts of HMP-2 Ser-47 with HMP-1 Asp-141 and HMP-2 Glu-50 are shown. Hydrogen bonding interactions are shown as *dashed lines*. *C,* non-polar packing interactions near Tyr-69 of HMP-2 are shown. *Dotted lines* represent distances of <4 Å.

difference may reflect the longer tail of E-cadherin *versus* HMR-1 (Ref. 21 and discussed in Ref. 52). The structural features of the HMP-2·HMP-1–binding interface, including the polar interactions between HMP-2 and the HMP-1 α1 helix, may enable constitutively strong binding in the presence or absence of HMR-1. The result is that in both the nematode and mammalian systems α-catenin binds to the cadherin·β-catenin complex with single nanomolar affinity, but the binding energetics are encoded differently.

Latent ability of HMP-1 to homodimerize provides insights into α-catenin evolution

The evolutionary origins of α-catenin functions beyond binding to β-catenin are unclear, especially regarding the functions of α-catenin homodimers (58). Our results shed light on the diversification of α-catenins with regard to homodimerization, which competes with β-catenin binding. Mammalian αE-catenin has a strong propensity to homodimerize, and there is evidence that homodimeric αE-catenin has roles away from junctions, including suppression of Arp2/3-mediated actin polymerization (26, 59). *Drosophila* α-catenin likewise seems to exist predominantly in a homodimeric form (60). In contrast, αE-catenin from zebrafish is monomeric (61), as is *Dictyostelium* α-catenin (62). αN-catenin seems to have its own characteristic feature, temperature-dependent dimerization. At 37 °C, αN-catenin readily forms a homodimer, although it can be purified as a monomer at 4 °C (13). Our results shed light on the structural requirements for constitutive homodimerization. *C. elegans* HMP-1 is predominantly monomeric even after overnight incubation at physiological temperature; however, HMP-1NΔ44 or HMP-1NΔ70, in which the N-terminal four-helix bundle is disrupted, shows a strong tendency to homodimerize in solution. Unlike mammalian αE-catenin, whose homodimeric form does not measurably bind to β-catenin, HMP-1NΔ44 binds weakly to HMP-2, with K_d of ~2 μM, and HMP-1Δ2–44::GFP is still able to rescue *hmp-1*(*zu278*), albeit weakly. Taken together, results across the animal kingdom suggest that α-catenins may have evolved independently multiple times to acquire their homodimerization abilities to fit specific demands in different organisms and that the α1 helix is crucial for masking this latent capability.

Conserved phosphorylatable residues in β-catenin are required for association with α-catenin

In addition to the important role of the α1 helix in mediating the α-catenin·β-catenin–binding interface, our work also demonstrates the crucial role of two specific amino acids in β-catenin *in vivo*. HMP-2 Ser-47 and Tyr-69 are homologous to the vertebrate β-catenin Thr-120 and Tyr-142, respectively. Phosphorylation at Tyr-142 of β-catenin has been shown to inhibit its ability to bind α-catenin (30, 32), likely because the introduction of a negatively charged phosphate group disrupts the predominantly hydrophobic interface between the two molecules (11, 12, 23). In contrast, the role of phosphorylation of Thr-120 has not been examined. Our work shows that phosphorylation of the amino acid homologous to Thr-120 of β-catenin could disrupt the interaction with α-catenin. Ser-47 and Tyr-69 of HMP-2 are located at the N- and the C-terminal ends, respectively, of the HMP-2 helix in the HMP-1·HMP-2 complex, similar to the positions of Thr-120 and Tyr-142 in the β-catenin·α-catenin complex (7, 13). It is compelling to speculate that this positioning allows for access by kinases to disrupt the HMP-2·HMP-1 association and therefore modulate CCC function. It is interesting that phosphomimetic mutants (S47E or Y69E) of HMP-2 show more severe defects *in vivo* than an HMP-1 Δα1 deletion mutant, whose affinity is ~20–50-fold weaker than that between a phosphomimetic mutant of HMP-2 and HMP-1 *in vitro*. This suggests that phosphorylation of HMP-2 plays other important regulatory roles besides the direct effects on HMP-1·HMP-2 binding during embryogenesis.

Although endogenous phosphorylation has not yet been observed at HMP-2 Ser-47 or Tyr-69 (63), it may be extremely difficult to detect whether it is only required transiently during dynamic junctional remodeling. The observation that HMP-2(S47A)::GFP and HMP-2(Y69F)::GFP constructs exhibit different junctional dynamics from wild-type HMP-2::GFP is consistent with the possibility that HMP-2 is endogenously phosphorylated at these sites. Although it is possible that the S47A and Y69F mutations may subtly alter HMP-2 protein folding in such a way as to reduce its junctional mobility, the fact that both non-phosphorylatable constructs show full affinity for HMP-1 *in vitro* and rescue *hmp-2*(*zu364*) to viability *in vivo* suggests that conformation of the mutant protein is not severely altered.

In conclusion, our *in vitro* and *in vivo* functional studies have definitively demonstrated the importance of α1 helix interactions in stabilizing the α-catenin·β-catenin–binding interface, and how phosphorylation of β-catenin can regulate its binding to α-catenin. Our results will enable future studies of the

Table 2
ITC measurement of HMP-1 binding to HMP-2 mutants

Proteins		K_D	ΔH	$T\Delta S$	ΔG
		nM	kcal mol^{-1}	kcal mol^{-1}	kcal mol^{-1}
HMP-1N	HMP-2 (13–678) (S47A)	1.0 ± 0.2	−16.2 ± 0.3	−3.9	−12.3
HMP-1N	HMP-2 (13–678) (S47E)	33 ± 9	−22.0 ± 0.5	−11.9	−10.1
HMP-1N	HMP-2 (13–678) (Y69F)	1.0 ± 0.05	−16.9 ± 0.07	−4.6	−12.3
HMP-1N	HMP-2 (13–678) (Y69E)	104 ± 22	−8.6 ± 0.2	0.9	−9.5

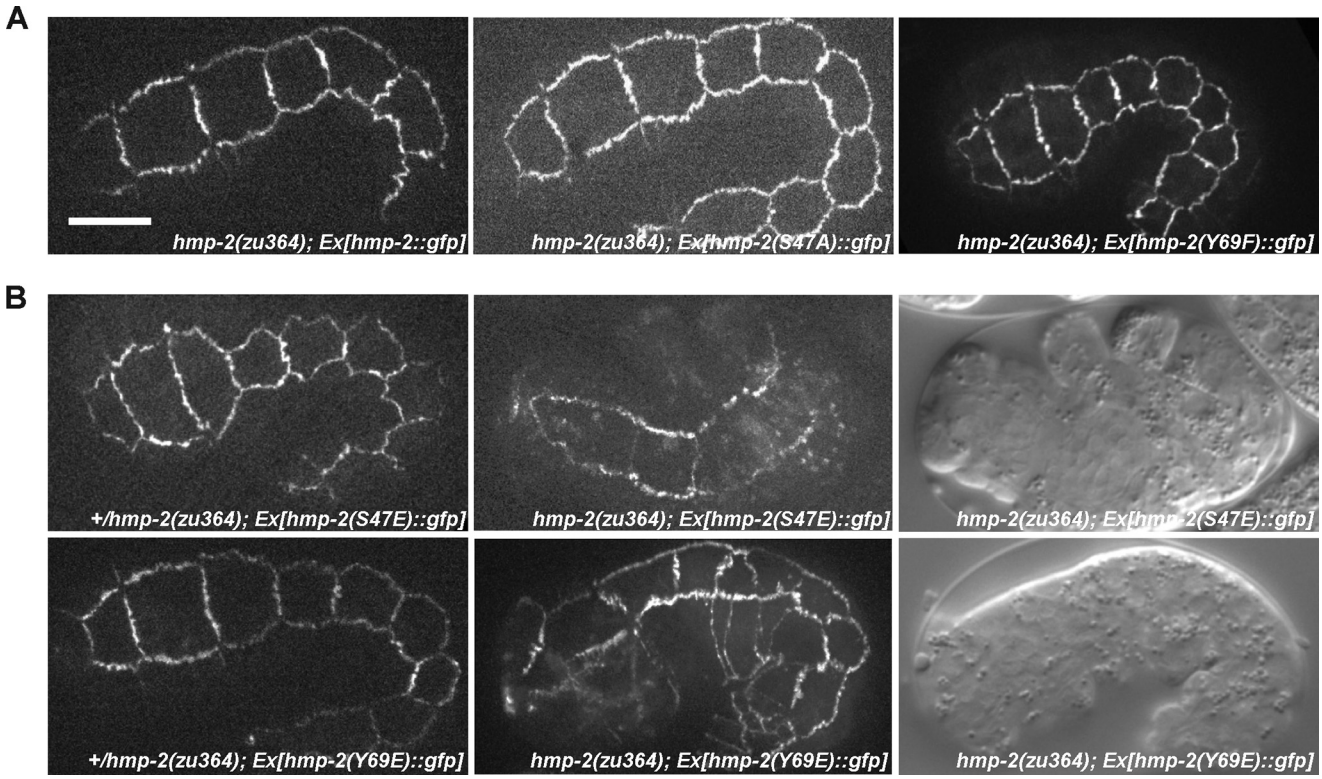

Figure 7. Regulation of HMP-2 function by Ser-47 and Tyr-69 *in vivo*. *A,* HMP-2(S47A)::GFP and HMP-2(Y69F)::GFP localize to junctions in a manner indistinguishable from wild-type HMP-2::GFP, and both are able to rescue the *hmp-2*(*zu364*) mutant allele. *Scale bar,* 10 μm. *B,* HMP-2(S47E)::GFP and HMP-2(Y69E)::GFP localize to junctions in +/*hmp-2*(*zu364*) embryos, but both of them fail to rescue *hmp-2*(*zu364*); embryos arrest during embryonic elongation.

detailed mechanisms by which cadherin-dependent cell–cell adhesion is modulated in all metazoans.

Experimental procedures

Protein expression and purification

HMP-1N, HMP-1NΔ44, HMP-2(36–79), HMP-2(13–678), HMP-2(36–678), and four mutants of HMP-2(13–678) (S47A, S47E, Y69E, and Y69F) were expressed in *Escherichia coli* Rosetta (DE3) cells, and full-length HMP-1 was expressed in *E. coli* BL21 (DE3) pLysS cells. Each cell was grown in Luria-Bertani (LB) medium with 100 μg ml^{-1} ampicillin and 34 μg ml^{-1} chloramphenicol until the A_{600} reached 0.6, and it was induced with 0.5 mM isopropyl β-D-1-thiogalactopyranoside. After overnight incubation at 20 °C, cells were harvested by centrifugation at 4000 rpm for 15 min at 4 °C and were resuspended with PBS containing DNase I (Roche Applied Science) and 1 mM PMSF. Resuspended cells were lysed with EmulsiFlex-C3 homogenizer (Avestin Inc.), and each cell lysate was centrifuged at 18,000 rpm for 30 min at 4 °C. The supernatant was collected and incubated for 1 h with glutathione-agarose beads (Pierce), which was pre-equilibrated with PBS. The column was washed with 10 column volumes of PBSTR buffer (1× PBS, 1 M NaCl, 5 mM DTT, 0.05% Tween 20) followed by 2 column volumes of cleavage buffer (30 mM Tris-HCl, pH 8.0, 100 mM NaCl, 2 mM DTT). To remove the GST tag, TEV protease was added into the column and incubated at 4 °C overnight. After TEV protease treatment, each protein was obtained in a flow-through fraction and loaded onto a HiTrap Q anion-exchange column (GE Healthcare), which had been pre-equilibrated with a buffer consisting of 20 mM Tris-HCl, pH 8.0, 20 mM NaCl, and 1 mM DTT. Protein was eluted by a linear gradient of 50–400 mM NaCl and further purified by Superdex 200 size-exclusion chromatography. To purify GST-HMP-2(36–79), instead of adding TEV protease, the elution buffer consisting of 50 mM Tris-HCl, pH 8.0, 0.1 M NaCl, and 20 mM reduced glutathione (GSH) was added into the G-agarose column, and eluted GST fusion protein was further purified using HiTrap Q anion-exchange column and Superdex 200 10/300 GL size-exclusion column (GE Healthcare).

ITC

Isothermal titration calorimetry was done using Nano ITC (TA Instruments, Inc.) at 25 °C in a buffer consisting of 20 mM HEPES, pH 8.0, 150 mM NaCl, and 1 mM DTT. For each mea-

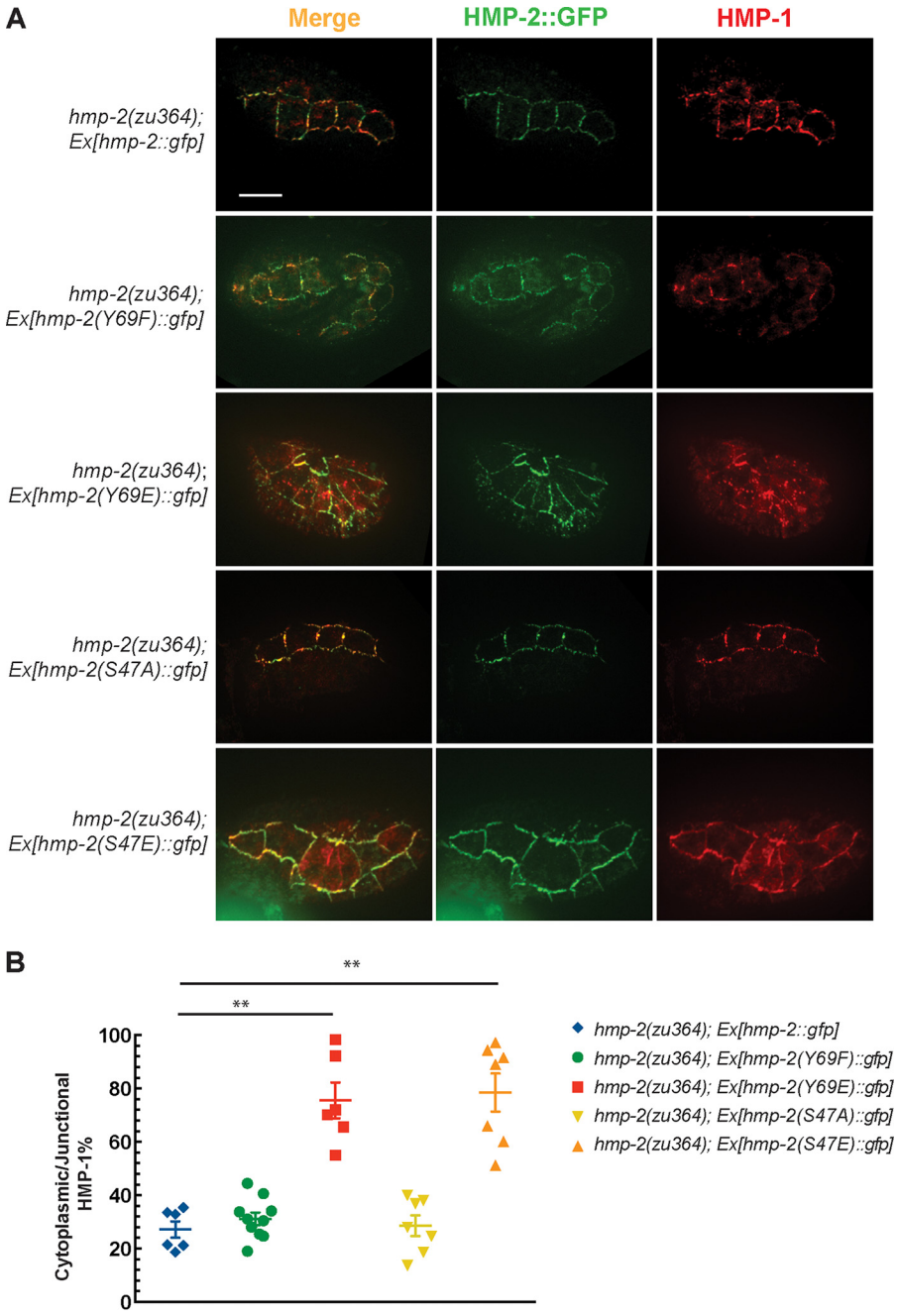

Figure 8. Regulation of HMP-1 junctional accumulation by HMP-2(Ser-47) and HMP-2(Tyr-69). *A,* in *hmp-2(zu364); hmp-2(S47E)::gfp* and *hmp-2(zu364); hmp-2(Y69E)::gfp* embryos, HMP-1 localizes more cytoplasmically compared with *hmp-2(zu364); hmp-2(S47A)::gfp* and *hmp-2(zu364); hmp-2(Y69F)::gfp* embryos, suggesting that HMP-2(S47E) and HMP-2(Y69E) have decreased binding affinity to HMP-1 compared with their non-phosphorylatable mutants *Scale bar,* 10 μm. *B,* quantitative results of HMP-1 localization in different strains from the images in *A*. Results are quantified as cytoplasmic/junctional HMP-1% (**, $p \leq 0.01$; Student's *t* test).

surement, 180–200 μM HMP-2 (GST-HMP-2(36–79), HMP-2(13–678), HMP-2(36–678), and HMP-2(13–678) mutants) was loaded onto the injector, and 10–40 μM HMP-1 (full-length HMP-1, HMP-1N, and HMP-1NΔ44) was loaded into the cell. Titration was carried out with 30–40 6–7-μl injections with 200-s intervals between injections. Data were analyzed by NanoAnalyze software.

Size-exclusion chromatography-multiangle light scattering (SEC-MALS)

SEC-MALS was performed with mini-DAWN TREOS detector (Wyatt Technology, Co.) in line with size-exclusion chromatography (GE Healthcare). 30 μM full-length HMP-1 was loaded on the column equilibrated with 20 mM HEPES, pH 7.5, 150 mM NaCl, and 0.1 mM tris(2-carboxyethyl)phosphine. Molecular weight was analyzed by Astra 6 (Wyatt Technology, Co.).

Circular dichroism spectroscopy

CD spectra were measured using a J-815 CD spectrometer (Jasco Analytical Instruments, Easton, MD). For thermal melting experiments, heat-induced changes were monitored at 222 nm for each of HMP-1 and HMP-1·HMP-2 complex samples in PBS buffer at a concentration of 0.2 mg/ml. Data were mea-

sured between 20 and 99 °C at a scan rate of 1 °C/min. All the spectra were corrected for solvent contribution.

Limited proteolysis

HMP-1 (40 μM) and HMP-1·HMP-2 complex (40 μM) were incubated with 0.02, 0.05, or 0.1 mg of endoprotease GluC (New England Biolabs) in 50 mM Tris-Cl, pH 8.0, buffer supplemented with 0.5 mM Glu-Glu dipeptide. Reactions were stopped at 15 and 45 min by adding SDS sample buffer. Samples were analyzed by SDS-PAGE and visualized by Coomassie Blue staining.

Crystallization, data collection, structure determination, and refinement of the HMP-1N·HMP-2(36–79) complex

The HMP-1N·HMP-2(36–79) complex was purified and crystallized as described earlier (64). Briefly, HMP-1N and HMP-2(36–79) were overexpressed separately as GST-fused forms and co-lysed and co-purified using a glutathione-affinity column, Mono Q ion-exchange column, and Superdex 200 size-exclusion column. Purified complex was concentrated to 11 mg ml^{-1} and crystallized in a hanging-drop plate with a reservoir solution containing 0.1 M citrate, pH 5.6, 0.2 M lithium sulfate, and 20% PEG 3350. Initial crystals were greatly improved by streak seeding.

Crystals of the HMP-1N·HMP-2(36–79) complex were cryoprotected by perfluoropolyether oil. A 1.6 Å resolution diffraction data set was collected at the Stanford Synchrotron Radiation Lightsource (SSRL) beamline 12-2 and processed using XDS and SCALA as described earlier (64). The structure was solved by molecular replacement using Phaser. The search model was the mouse βα-catenin chimeric protein structure (PDB code 1DOW), and a solution was obtained and refined to give initial R_{work} and R_{free} values of 49 and 54%, respectively. Several cycles of refinement and manual rebuilding were performed using PHENIX and Coot, respectively. The refinement statistics are shown in Table 3. The final model consists of HMP-1 residues 13–260 and HMP-2 residues 46–72. Coordinates and structure factors have been deposited in the Protein Data Bank under accession code 5XA5.

Computational modeling

The HMP-1·HMP-2 complex structure without neighboring molecules that make crystal contacts was relaxed by iterative short molecular dynamics simulations with subsequent side-chain repacking steps. The energy function used for relaxation comprised molecular mechanics energy terms and knowledge-based terms (65, 66). Additional restraints were applied to avoid drift away from the initial structure, as in typical relaxation (65–67). After relaxation, the lowest-energy structure among the generated 48 models was selected.

DNA constructs and strains used

hmp-1::gfp deletion mutants and *hmp-2* phosphomutants were generated via site-directed PCR mutagenesis of pJS434 ($P_{hmp\text{-}1}$:: *hmp-1::gfp*) and pTDL34($P_{hmp\text{-}2}$:: *hmp-2::gfp*). *hmp-1Δ2–44::gfp* primers are as follows: XS9-2, 5′-CAA ACT ACT GAA GGA CTT GTC G-3′ (forward), and XS10-2, 5′-CAT TCT GAA AAT TAA TAA AAT TGA AAA TTC-3-′ (reverse).

Table 3
Data collection and refinement statistics
r.m.s.d. is root mean square deviation.

Data collection	
Space group	$P3_121$
Unit cell parameters	
a, b, c (Å)	57.1, 57.1, 155.4
Resolution (Å) (last shell)	40–1.6 (1.67–1.60)
Completeness (%)	99.7 (99.0)
Redundancy	5.3 (5.0)
$\langle I/\sigma(I)\rangle$	24.3 (3.7)
R_{merge} [a]	0.027 (0.36)
$CC_{½}$ [b]	0.999 (0.886)
Refinement	
No. of reflections working set (test set)	39,608 (3775)
R_{cryst}/R_{free} [c]	0.19/0.23
Bond length r.m.s.d. from ideal (Å)	0.003
Bond angle r.m.s.d. from ideal (°)	0.75
Ramachandran analysis[d]	
% favored regions	95.8
% allowed regions	4.2
% outliers	0.0

[a] $R_{merge} = \Sigma_h\Sigma_i|I_{ih}\langle I_h\rangle|\Sigma_h\Sigma_i(h)$, where $I(h)$ is the ith measurement of reflection h, and $\langle I(h)\rangle$ is the weighted mean of all measurements of h.
[b] $CC_{½}$ is Pearson correlation coefficient between random half-datasets (68).
[c] $R = \Sigma_h||F_{obs}(h)| - |F_{calc}(h)||/\Sigma_h|F_{obs}(h)|$. R_{cryst} and R_{free} were calculated using the working and test reflection sets, respectively.
[d] Data are as defined in MolProbity.

hmp-1Δ47–71::gfp primers are as follows: XS34, 5′-TGC CCA ATT GCA AAC AGT GAT-3′ (forward), and XS35, 5′-AGT TTG TCC AGG TTT TAA CGG AAA C-3-′ (reverse). The *hmp-1Δ79–106::gfp* primers are as follows: XS36, 5′-GTC AGA GAT TCA ACT TCA ACA AAC AAA-3′ (forward), and XS37, 5′-ATC ACT GTT TGC AAT TGG GCA T-3′ (reverse). The *hmp-1Δ113–141::gfp* primers are as follows: XS39, 5′-GTA AAA GTG ATA GTT GAT AAA GTA GAT GAA GTT-3-′ (forward), and XS40, 5′-TGA AGT TGA ATC TCT GAC AAA ATC T-3-′ (reverse). The *hmp-2*(*S47*) mutagenesis primers are as follows: S47A F01, 5′-GCC ATC GTC GAA ATG ATG CAA-3′, and S47EF01 5′-GAA ATC GTC GAA ATG ATG CAA-3′. Both forward primers were paired with S47R 5′-TGT AGT TGA ATT TGT GGC TTC TGC-3′. The Tyr-69 mutagenesis primers are as follows: Y69F F02, 5′-TTC GAA GGA TCA AAC GAT ATG TCA-3′, and Y69E F02, 5′-GAG GAA GGA TCA AAC GAT ATG TCA-3′. Both forward primers paired with Tyr-69 R2 5′-GGT TAG AAG ATC CAT AAC TGA TTG-3′.

The following strains were used in this work: SU402 (*hmp-1*(*zu278*) V; jcEx110[*hmp-1::gfp*]), SU370 (+/*nT1*(*qIS51*) IV; *hmp-1*(*zu278*)/*nT1*(*qIS51*) V), SU814 (*hmp-1*(*zu278*) V; jcEX271[HMP-1Δ2–44::gfp]); SU771 (N2; jcEx259[*hmp-1Δ47-71::gfp*]); SU818(+/*hmp-1*(*zu278*) V; jcEx275 [*hmp-1Δ79-106::gfp*]); SU813 (+/*hmp-1*(*zu278*) V; jcEx275 [*hmp-1Δ113-141::gfp*]), JJ1068 (*hmp-2*(*zu364*)/hIn1[unc-54(h1040)] I), SU570 (*hmp-2*(*zu364*) I; *jcEx188*[*hmp-2*(*Y69F*)*::gfp*]), SU574 (*hmp-2*(*zu364*)/*hIn1*[*unc-54*(*h1040*)] I; *jcEx189*[*hmp-2*(*Y69E*)*::gfp*]), SU593 (*hmp-2*(*zu364*)/*hIn1*[*unc-54*(*h1040*)] I; *jcEx193*[*hmp-2*(*S47E*)*::gfp*]), SU594 (*hmp-2*(*zu364*) I; *jcEx194*[*hmp-2*(*S47A*)*::gfp*]), SU569 (*hmp-2*(*zu364*) I; *jcEx187* [*hmp-2::gfp*]).

All *hmp-1::gfp* constructs were injected at 1 ng/μl with 79 ng/μl pRF4[*rol-6*(*su1006*)] and 20 ng/μl F35D3. *hmp-2::gfp* constructs were injected at 20 ng/μl with 80 ng/μl pRF4[*rol-6*(*su1006*)] and 20 ng/μl F35D3. All strains were maintained at 20 °C and fed OP50 bacteria on standard NGM plates (69).

Immunostaining

Embryos were isolated from gravid hermaphrodites with 0.5% NaOCl in 250 mM NaOH for 5 min followed by three washes in distilled deionized water. For antibody staining, embryos were mounted on poly-L-lysine-coated ring slides and covered with a coverslip. Slides were quick frozen for 10 min on dry ice and then the coverslips were removed with a razor blade. Slides were immediately transferred to methanol at −20 °C for 5 min, then acetone at −20 °C for 5 min, and PBST at room temperature for 5 min, followed by two additional PBST washes. Embryos were incubated with 1:4000 rabbit anti-HMP-1 and 1:500 mouse anti-GFP in 5% milk/PBST in the dark overnight at 4 °C. Slides were washed three times with PBST and then incubated in the dark for 4 h at room temperature with 1:50 anti-rabbit Texas Red and 1:50 anti-mouse FITC in 5% milk/PBST. Slides were washed three times with PBST before being covered with antifade reagent and sealed with nail polish.

Imaging

Embryos were isolated from gravid hermaphrodites, mounted on a 5% agarose slide, and aged at 20–25 °C until the onset of morphogenesis. For four-dimensional differential interference contrast microscopy, embryos were imaged using 1-μm slice spacing at 3-min intervals using a Nikon Eclipse E600 microscope with a ×60/1.45 NA oil objective at 20 °C with a Macintosh computer running ImageJ using custom macros/plugins. For fluorescent imaging, a PerkinElmer Life Sciences UltraView spinning disk confocal microscope and Micromanager software, using a Nikon Eclipse E600 microscope and Hamamatsu ORCA-ER camera, were used to collect images of GFP-expressing embryos, using 0.5-μm slices at 3-min intervals with a ×60/1.45 NA oil objective at 20 °C. Antibody staining (0.6-μm slices) images were collected with the same confocal microscope using a ×100/1.45 NA oil objective.

FRAP

Transgenic embryos were isolated from gravid hermaphrodites, mounted on 5% agarose slide, and aged at 20 °C for 4 h or until the onset of elongation. The FRAP experiments were then performed as described in our previous research (50).

Author contributions—X. S. and T. L. performed *in vivo* rescue experiments and related cloning. H. K. conducted *in vitro* biochemical experiments, including protein purification, MALS, and ITC experiments. H. J. C. performed X-ray crystallographic experiments. G. R. L. and C. S. performed computational modeling experiments. H. J. C., W. I. W., and J. H. outlined the manuscript; X. S., T. L., H. J. C., and J. H. wrote the paper. H. J. C., W. I. W., and J. H. conceived and directed the study. All authors discussed the results and approved the final version of the manuscript.

Acknowledgments—Members of the Hardin laboratory thank Bethany Lucas for helpful discussions. Use of the Stanford Synchrotron Radiation Lightsource, SLAC National Accelerator Laboratory, is supported by the United States Department of Energy, Office of Science, Office of Basic Energy Sciences under Contract No. DE-AC02–76SF00515. The SSRL Structural Molecular Biology Program is supported by Department of Energy Office of Biological and Environmental Research and by NIGMS Grant P41GM103393 from the National Institutes of Health.

References

1. Gumbiner, B. M. (1996) Cell adhesion: the molecular basis of tissue architecture and morphogenesis. *Cell* **84,** 345–357
2. Benjamin, J. M., and Nelson, W. J. (2008) Bench to bedside and back again: molecular mechanisms of α-catenin function and roles in tumorigenesis. *Semin. Cancer Biol.* **18,** 53–64
3. Huber, M. A., Kraut, N., and Beug, H. (2005) Molecular requirements for epithelial-mesenchymal transition during tumor progression. *Curr. Opin. Cell Biol.* **17,** 548–558
4. Franke, W. W. (2009) Discovering the molecular components of intercellular junctions–a historical view. *Cold Spring Harb. Perspect. Biol.* **1,** a003061
5. Ozawa, M., Baribault, H., and Kemler, R. (1989) The cytoplasmic domain of the cell adhesion molecule uvomorulin associates with three independent proteins structurally related in different species. *EMBO J.* **8,** 1711–1717
6. Pokutta, S., Drees, F., Takai, Y., Nelson, W. J., and Weis, W. I. (2002) Biochemical and structural definition of the L-afadin- and actin-binding sites of α-catenin. *J. Biol. Chem.* **277,** 18868–18874
7. Pokutta, S., and Weis, W. I. (2000) Structure of the dimerization and β-catenin-binding region of α-catenin. *Mol. Cell* **5,** 533–543
8. Buckley, C. D., Tan, J., Anderson, K. L., Hanein, D., Volkmann, N., Weis, W. I., Nelson, W. J., and Dunn, A. R. (2014) Cell adhesion. The minimal cadherin-catenin complex binds to actin filaments under force. *Science* **346,** 1254211
9. Rimm, D. L., Koslov, E. R., Kebriaei, P., Cianci, C. D., and Morrow, J. S. (1995) α1(E)-catenin is an actin-binding and -bundling protein mediating the attachment of F-actin to the membrane adhesion complex. *Proc. Natl. Acad. Sci. U.S.A.* **92,** 8813–8817
10. Herrenknecht, K., Ozawa, M., Eckerskorn, C., Lottspeich, F., Lenter, M., and Kemler, R. (1991) The uvomorulin-anchorage protein α-catenin is a vinculin homologue. *Proc. Natl. Acad. Sci. U.S.A.* **88,** 9156–9160
11. Ishiyama, N., Tanaka, N., Abe, K., Yang, Y. J., Abbas, Y. M., Umitsu, M., Nagar, B., Bueler, S. A., Rubinstein, J. L., Takeichi, M., and Ikura, M. (2013) An autoinhibited structure of α-catenin and its implications for vinculin recruitment to adherens junctions. *J. Biol. Chem.* **288,** 15913–15925
12. Rangarajan, E. S., and Izard, T. (2012) The cytoskeletal protein α-catenin unfurls upon binding to vinculin. *J. Biol. Chem.* **287,** 18492–18499
13. Pokutta, S., Choi, H. J., Ahlsen, G., Hansen, S. D., and Weis, W. I. (2014) Structural and thermodynamic characterization of cadherin. β-Catenin·α-catenin complex formation. *J. Biol. Chem.* **289,** 13589–13601
14. Imamura, Y., Itoh, M., Maeno, Y., Tsukita, S., and Nagafuchi, A. (1999) Functional domains of α-catenin required for the strong state of cadherin-based cell adhesion. *J. Cell Biol.* **144,** 1311–1322
15. Choi, H. J., Pokutta, S., Cadwell, G. W., Bobkov, A. A., Bankston, L. A., Liddington, R. C., and Weis, W. I. (2012) αE-catenin is an autoinhibited molecule that coactivates vinculin. *Proc. Natl. Acad. Sci. U.S.A.* **109,** 8576–8581
16. Watabe-Uchida, M., Uchida, N., Imamura, Y., Nagafuchi, A., Fujimoto, K., Uemura, T., Vermeulen, S., van Roy, F., Adamson, E. D., and Takeichi, M. (1998) α-Catenin-vinculin interaction functions to organize the apical junctional complex in epithelial cells. *J. Cell Biol.* **142,** 847–857
17. Thomas, W. A., Boscher, C., Chu, Y. S., Cuvelier, D., Martinez-Rico, C., Seddiki, R., Heysch, J., Ladoux, B., Thiery, J. P., Mege, R. M., and Dufour, S. (2013) α-Catenin and vinculin cooperate to promote high E-cadherin-based adhesion strength. *J. Biol. Chem.* **288,** 4957–4969
18. Yonemura, S., Wada, Y., Watanabe, T., Nagafuchi, A., and Shibata, M. (2010) α-Catenin as a tension transducer that induces adherens junction development. *Nat. Cell Biol.* **12,** 533–542
19. Choi, H. J., Loveless, T., Lynch, A. M., Bang, I., Hardin, J., and Weis, W. I. (2015) A conserved phosphorylation switch controls the interaction between cadherin and β-catenin *in vitro* and *in vivo*. *Dev. Cell* **33,** 82–93
20. Choi, H. J., Huber, A. H., and Weis, W. I. (2006) Thermodynamics of β-catenin-ligand interactions: the roles of the N- and C-terminal tails in modulating binding affinity. *J. Biol. Chem.* **281,** 1027–1038

21. Huber, A. H., and Weis, W. I. (2001) The structure of the β-catenin/E-cadherin complex and the molecular basis of diverse ligand recognition by β-catenin. *Cell* **105,** 391–402
22. Stappert, J., and Kemler, R. (1994) A short core region of E-cadherin is essential for catenin binding and is highly phosphorylated. *Cell Adhes. Commun.* **2,** 319–327
23. Aberle, H., Schwartz, H., Hoschuetzky, H., and Kemler, R. (1996) Single amino acid substitutions in proteins of the armadillo gene family abolish their binding to α-catenin. *J. Biol. Chem.* **271,** 1520–1526
24. Huber, O., Krohn, M., and Kemler, R. (1997) A specific domain in α-catenin mediates binding to β-catenin or plakoglobin. *J. Cell Sci.* **110,** 1759–1765
25. Aberle, H., Butz, S., Stappert, J., Weissig, H., Kemler, R., and Hoschuetzky, H. (1994) Assembly of the cadherin-catenin complex *in vitro* with recombinant proteins. *J. Cell Sci.* **107,** 3655–3663
26. Drees, F., Pokutta, S., Yamada, S., Nelson, W. J., and Weis, W. I. (2005) α-Catenin is a molecular switch that binds E-cadherin-β-catenin and regulates actin-filament assembly. *Cell* **123,** 903–915
27. Yamada, S., Pokutta, S., Drees, F., Weis, W. I., and Nelson, W. J. (2005) Deconstructing the cadherin-catenin-actin complex. *Cell* **123,** 889–901
28. Takeichi, M. (2014) Dynamic contacts: rearranging adherens junctions to drive epithelial remodelling. *Nat. Rev. Mol. Cell Biol.* **15,** 397–410
29. Daugherty, R. L., and Gottardi, C. J. (2007) Phospho-regulation of β-catenin adhesion and signaling functions. *Physiology* **22,** 303–309
30. David, M. D., Yeramian, A., Duñach, M., Llovera, M., Cantí, C., de Herreros, A. G., Comella, J. X., and Herreros, J. (2008) Signalling by neurotrophins and hepatocyte growth factor regulates axon morphogenesis by differential β-catenin phosphorylation. *J. Cell Sci.* **121,** 2718–2730
31. Lilien, J., Balsamo, J., Arregui, C., and Xu, G. (2002) Turn-off, drop-out: functional state switching of cadherins. *Dev. Dyn.* **224,** 18–29
32. Piedra, J., Miravet, S., Castaño, J., Pálmer, H. G., Heisterkamp, N., García de Herreros, A., and Duñach, M. (2003) p120 Catenin-associated Fer and Fyn tyrosine kinases regulate β-catenin Tyr-142 phosphorylation and β-catenin-α-catenin interaction. *Mol. Cell Biol.* **23,** 2287–2297
33. Roura, S., Miravet, S., Piedra, J., García de Herreros, A., and Duñach, M. (1999) Regulation of E-cadherin/catenin association by tyrosine phosphorylation. *J. Biol. Chem.* **274,** 36734–36740
34. Xu, G., Craig, A. W., Greer, P., Miller, M., Anastasiadis, P. Z., Lilien, J., and Balsamo, J. (2004) Continuous association of cadherin with β-catenin requires the non-receptor tyrosine-kinase Fer. *J. Cell Sci.* **117,** 3207–3219
35. Müller, T., Choidas, A., Reichmann, E., and Ullrich, A. (1999) Phosphorylation and free pool of β-catenin are regulated by tyrosine kinases and tyrosine phosphatases during epithelial cell migration. *J. Biol. Chem.* **274,** 10173–10183
36. Rhee, J., Mahfooz, N. S., Arregui, C., Lilien, J., Balsamo, J., and VanBerkum, M. F. (2002) Activation of the repulsive receptor roundabout inhibits N-cadherin-mediated cell adhesion. *Nat. Cell Biol.* **4,** 798–805
37. Taddei, M. L., Chiarugi, P., Cirri, P., Buricchi, F., Fiaschi, T., Giannoni, E., Talini, D., Cozzi, G., Formigli, L., Raugei, G., and Ramponi, G. (2002) β-Catenin interacts with low-molecular-weight protein tyrosine phosphatase leading to cadherin-mediated cell–cell adhesion increase. *Cancer Res.* **62,** 6489–6499
38. McEwen, A. E., Maher, M. T., Mo, R., and Gottardi, C. J. (2014) E-cadherin phosphorylation occurs during its biosynthesis to promote its cell surface stability and adhesion. *Mol. Biol. Cell* **25,** 2365–2374
39. Tamada, M., Farrell, D. L., and Zallen, J. A. (2012) Abl regulates planar polarized junctional dynamics through β-catenin tyrosine phosphorylation. *Dev. Cell* **22,** 309–319
40. van Veelen, W., Le, N. H., Helvensteijn, W., Blonden, L., Theeuwes, M., Bakker, E. R., Franken, P. F., van Gurp, L., Meijlink, F., van der Valk, M. A., Kuipers, E. J., Fodde, R., and Smits, R. (2011) β-Catenin tyrosine 654 phosphorylation increases Wnt signalling and intestinal tumorigenesis. *Gut* **60,** 1204–1212
41. Brembeck, F. H., Schwarz-Romond, T., Bakkers, J., Wilhelm, S., Hammerschmidt, M., and Birchmeier, W. (2004) Essential role of BCL9–2 in the switch between β-catenin's adhesive and transcriptional functions. *Genes Dev.* **18,** 2225–2230
42. Tominaga, J., Fukunaga, Y., Abelardo, E., and Nagafuchi, A. (2008) Defining the function of β-catenin tyrosine phosphorylation in cadherin-mediated cell–cell adhesion. *Genes Cells* **13,** 67–77
43. Chen, X. L., Nam, J. O., Jean, C., Lawson, C., Walsh, C. T., Goka, E., Lim, S. T., Tomar, A., Tancioni, I., Uryu, S., Guan, J. L., Acevedo, L. M., Weis, S. M., Cheresh, D. A., and Schlaepfer, D. D. (2012) VEGF-induced vascular permeability is mediated by FAK. *Dev. Cell* **22,** 146–157
44. Du, C., Jaggi, M., Zhang, C., aβd Balaji, K. C. (2009) Protein kinase D1-mediated phosphorylation and subcellular localization of β-catenin. *Cancer Res.* **69,** 1117–1124
45. Du, C., Zhang, C., Li, Z., Biswas, M. H., and Balaji, K. C. (2012) β-Catenin phosphorylated at threonine 120 antagonizes generation of active β-catenin by spatial localization in trans-Golgi network. *PLoS ONE* **7,** e33830
46. Jaggi, M., Chauhan, S. C., Du, C., and Balaji, K. C. (2008) Bryostatin 1 modulates β-catenin subcellular localization and transcription activity through protein kinase D1 activation. *Mol. Cancer Ther.* **7,** 2703–2712
47. Pettitt, J., Cox, E. A., Broadbent, I. D., Flett, A., and Hardin, J. (2003) The *Caenorhabditis elegans* p120 catenin homologue, JAC-1, modulates cadherin-catenin function during epidermal morphogenesis. *J. Cell Biol.* **162,** 15–22
48. Costa, M., Raich, W., Agbunag, C., Leung, B., Hardin, J., and Priess, J. R. (1998) A putative catenin-cadherin system mediates morphogenesis of the *Caenorhabditis elegans* embryo. *J. Cell Biol.* **141,** 297–308
49. Kwiatkowski, A. V., Maiden, S. L., Pokutta, S., Choi, H. J., Benjamin, J. M., Lynch, A. M., Nelson, W. J., Weis, W. I., and Hardin, J. (2010) *In vitro* and *in vivo* reconstitution of the cadherin-catenin-actin complex from *Caenorhabditis elegans*. *Proc. Natl. Acad. Sci. U.S.A.* **107,** 14591–14596
50. Maiden, S. L., Harrison, N., Keegan, J., Cain, B., Lynch, A. M., Pettitt, J., and Hardin, J. (2013) Specific conserved C-terminal amino acids of *Caenorhabditis elegans* HMP-1/α-catenin modulate F-actin binding independently of vinculin. *J. Biol. Chem.* **288,** 5694–5706
51. Koslov, E. R., Maupin, P., Pradhan, D., Morrow, J. S., and Rimm, D. L. (1997) α-Catenin can form asymmetric homodimeric complexes and/or heterodimeric complexes with β-catenin. *J. Biol. Chem.* **272,** 27301–27306
52. Kang, H., Bang, I., Jin, K. S., Lee, B., Lee, J., Shao, X., Heier, J. A., Kwiatkowski, A. V., Nelson, W. J., Hardin, J., Weis, W. I., and Choi, H. J. (2017) Structural and functional characterization of *Caenorhabditis elegans* α-catenin reveals constitutive binding to β-catenin and F-actin. *J. Biol. Chem.* **292,** 7077–7086
53. Izard, T., Evans, G., Borgon, R. A., Rush, C. L., Bricogne, G., and Bois, P. R. (2004) Vinculin activation by talin through helical bundle conversion. *Nature* **427,** 171–175
54. Papagrigoriou, E., Gingras, A. R., Barsukov, I. L., Bate, N., Fillingham, I. J., Patel, B., Frank, R., Ziegler, W. H., Roberts, G. C., Critchley, D. R., and Emsley, J. (2004) Activation of a vinculin-binding site in the talin rod involves rearrangement of a five-helix bundle. *EMBO J.* **23,** 2942–2951
55. Korswagen, H. C., Herman, M. A., and Clevers, H. C. (2000) Distinct β-catenins mediate adhesion and signalling functions in *C. elegans*. *Nature* **406,** 527–532
56. Natarajan, L., Witwer, N. E., and Eisenmann, D. M. (2001) The divergent *Caenorhabditis elegans* β-catenin proteins BAR-1, WRM-1 and HMP-2 make distinct protein interactions but retain functional redundancy *in vivo*. *Genetics* **159,** 159–172
57. Phillips, B. T., and Kimble, J. (2009) A new look at TCF and β-catenin through the lens of a divergent *C. elegans* Wnt pathway. *Dev. Cell* **17,** 27–34
58. Miller, P. W., Clarke, D. N., Weis, W. I., Lowe, C. J., and Nelson, W. J. (2013) The evolutionary origin of epithelial cell–cell adhesion mechanisms. *Curr. Top. Membr.* **72,** 267–311
59. Maiden, S. L., and Hardin, J. (2011) The secret life of α-catenin: moonlighting in morphogenesis. *J. Cell Biol.* **195,** 543–552
60. Desai, R., Sarpal, R., Ishiyama, N., Pellikka, M., Ikura, M., and Tepass, U. (2013) Monomeric α-catenin links cadherin to the actin cytoskeleton. *Nat. Cell Biol.* **15,** 261–273
61. Miller, P. W., Pokutta, S., Ghosh, A., Almo, S. C., Weis, W. I., Nelson, W. J., and Kwiatkowski, A. V. (2013) *Danio rerio* αE-catenin is a monomeric

F-actin binding protein with distinct properties from *Mus musculus* αE-catenin. *J. Biol. Chem.* **288,** 22324–22332
62. Dickinson, D. J., Nelson, W. J., and Weis, W. I. (2011) A polarized epithelium organized by β- and α-catenin predates cadherin and metazoan origins. *Science* **331,** 1336–1339
63. Callaci, S., Morrison, K., Shao, X., Schuh, A. L., Wang, Y., Yates, J. R., 3rd., Hardin, J., and Audhya, A. (2015) Phosphoregulation of the *C. elegans* cadherin-catenin complex. *Biochem. J.* **472,** 339–352
64. Kang, H., Bang, I., Weis, W. I., and Choi, H. J. (2016) Purification, crystallization and initial crystallographic analysis of the α-catenin homologue HMP-1 from *Caenorhabditis elegans*. *Acta Crystallogr. F Struct. Biol. Commun.* **72,** 234–239
65. Heo, L., Park, H., and Seok, C. (2013) GalaxyRefine: Protein structure refinement driven by side-chain repacking. *Nucleic Acids Res.* **41,** W384–W388
66. Lee, G. R., Heo, L., and Seok, C. (2016) Effective protein model structure refinement by loop modeling and overall relaxation. *Proteins* **84,** 293–301
67. Park, H., Lee, G. R., Heo, L., and Seok, C. (2014) Protein loop modeling using a new hybrid energy function and its application to modeling in inaccurate structural environments. *PLoS ONE* **9,** e113811
68. Diederichs, K., and Karplus, P. A. (2013) Better models by discarding data? *Acta Crystallogr. D Biol. Crystallogr.* **69,** 1215–1222
69. Brenner, S. (1974) The genetics of *Caenorhabditis elegans*. *Genetics* **77,** 71–94